This is a repository copy of *An analysis of the influence of high-frequency ripple currents on dynamic charge acceptance in lead-acid batteries*.

An Analysis of the Influence of High-Frequency Ripple Currents on Dynamic Charge Acceptance in Lead-Acid Batteries

M J Smith*, D T Gladwin, D A Stone

Centre for Research into Electrical Energy Storage & Applications,
Department of Electronic and Electrical Engineering,
The University of Sheffield,
Solly Street, Sheffield, S1 4DE, UK

Abstract

This paper presents the results of an experimental analysis of the influence of high-frequency injected ripple currents on the Dynamic Charge Acceptance (DCA) performance of lead-acid batteries. A wide-bandwidth battery model, derived from real-world data is described, this being a hybrid of the standard Randles model and a high-frequency model previously presented in literature. A bespoke test procedure is introduced, based on the existing DCA Short Test profile (EN50342-6). The results demonstrate that the injection of ripple currents can significantly improve charge acceptance, whilst having no appreciable effect on the State of Charge (SoC) of the battery. This study further demonstrates the importance of knowledge of the impedance spectrum of the battery if the improvements in DCA performance are to be achieved with maximum efficiency and effectiveness.

Keywords: Automotive battery; Dynamic charge acceptance; Hybrid Electric Vehicle; Ripple current; Test regime

1. Introduction

1.1. Automotive Battery Use

There has been a major shift over recent years in the use of batteries in automotive applications. Traditionally the battery has been used exclusively as an auxiliary energy store, nowadays the use of the battery purely for starting, lighting and ignition (SLI) is becoming increasingly rare. Environmental and economic concerns mean the internal combustion engine is run less, utilising either start-stop or hybrid electric vehicle (HEV) technology; or eliminated altogether in the case of fully electric vehicles (EV). Concurrently, vehicles are becoming more power-hungry, with increasingly complex on-board driver aids, entertainment and HVAC systems. These changes

---

*Corresponding author
Email address:* `matt.j.smith@sheffield.ac.uk` (M J Smith)

make the performance of the battery more fundamental than ever to the overall performance of the vehicle.

These developments result in battery being used in fundamentally different ways, depending on the type of vehicle in which it is installed. In EVs, where the battery is the only source of traction power, the operation becomes very cyclic; the battery is charged from an external power supply and becomes discharged as the vehicle is driven. Whilst some energy can be recovered by regenerative braking, this process can never be 100 % efficient, eventually the battery must once again be charged from an external source.

This results in the battery being subjected to repeating cycles of charge and discharge, and the performance of the vehicle being primarily limited by the amount of energy which can be stored and the rate at which it can be recharged. For this duty, lithium-based batteries are the technology of choice. Although such batteries have relatively high initial costs these are offset by the benefits of the high energy density, long cycle-life and fast charge capability of lithium cells.

An alternative approach is taken by HEVs. Here the internal combustion engine is retained and the battery is used to augment its power and store energy from regenerative braking. Although there are several possible drive-train configurations [1] for HEVs, they all allow for the vehicle to be driven using the internal combustion engine or the batteries alone, or the both combined.

This approach means the duty applied to the batteries is far less predictable than in an EV and characterised by short, high-rate pulses of either charge or discharge across a wide range of State of Charge (SoC). In this situation the ability of the battery to operate reliably under these high-rate, partial SoC (HRPSoC) conditions becomes more important than absolute capacity. In addition as the battery must share a limited space within the vehicle with the engine, its physical size must be less than that of an EV battery. These factors combine to allow lead-acid batteries to remain a viable proposition for HEVs [2].

1.2. Dynamic Charge Acceptance

A key area of interest stemming from this change has been the study of Dynamic Charge Acceptance (DCA) in batteries. This is important because the nature of the operating environment for HEV batteries means they are often subjected to very high rates of charge, up to 30 times the 1-hour rate (C_1), during regenerative braking [3]. Overall battery effectiveness under these conditions is determined to a large extent by how well they are able to accept the energy available from these high-current pulses. Better DCA performance means more charge accepted, which in turn equates to more efficient energy recovery.

Increased understanding of DCA performance has been identified as an important contributor to the continuing development of automotive batteries [4]. A standard test procedure exists for characterising the DCA performance of batteries [5], and detailed studies have been undertaken

to determine how test parameters and external conditions affect DCA performance [6, 7, 8].

Whilst most efforts have focussed on DCA for automotive applications, the underlying principle has much wider applications and is important in any system where it is desirable for a battery to accept charge in a time-limited fashion. Such applications include grid-connected storage systems, particularly when operating in Enhanced Frequency Response (EFR) mode, and smaller scale renewable energy systems. Clearly then, a greater understanding of the factors influencing DCA performance, and methods for improving it could have broad applications across the whole energy storage sector.

1.3. DCA Improvement Methods

Previous work by the authors, and others, has identified four main factors which influence the DCA performance of batteries, and which therefore may provide scope for improving it. These factors: SoC, temperature, history and microcycling are now considered in turn.

The SoC of the battery has a very significant effect on DCA performance, with much greater levels of charge acceptance being possible at low SoC. Intuitively this makes sense as the main physical limitation on charge acceptance is the terminal voltage of the battery, a battery at a lower SoC will have a lower terminal voltage, and therefore have a greater ability to accept charge than one at a higher SoC. In practice, however, it is rarely practical to take advantage of this. Whilst it is possible to arbitrarily limit the maximum SoC of the battery to achieve better DCA performance, this results in the battery storing less energy than it is capable of. To achieve the same energy storage ability, would thus require the use of a larger battery. Clearly, in automotive applications where the size and weight of the battery pack is fundamentally limited, this approach is unsuitable.

Battery temperature is also important in DCA performance, with higher temperatures promoting improved charge acceptance [6]. Again this is to be expected as the underlying electrochemical reactions governing battery performance obey the Arrhenius equation[9], and thus proceed more easily at higher temperatures. Again, though, it is difficult to take advantage of this effect as the high currents to which automotive batteries are subjected cause internal heating due to losses within the battery. To avoid excessive temperatures being reached the batteries are cooled to around $40\ ^\circ C$ – $50\ ^\circ C$, allowing the temperature to rise above this level would improve DCA performance, but would also risk long term damage being caused in the process.

The history of the battery, whether it has been recently charged or discharged, also has a large influence on DCA performance, with higher charge acceptance observed when the battery has discharge history [6, 10, 11], due to the differing electrochemical environment with the battery between charge and discharge. Clearly, there is no way to reliably take advantage of this effect, as it is impossible to predict the operations which will be performed on the battery in advance.

3

Without the ability to reliably predict when a discharge will occur, and thus when the battery will be capable of increased DCA performance the system must always default to assuming worst-case DCA performance and therefore risk recapturing less energy than is actually available.

1.4. DCA Improvement by Applied Ripple Current

The final method for influencing DCA performance is microcycling, which involves repeatedly applying short-duration charges and discharges to the battery. This has been shown experimentally by the authors to improve charge acceptance in both lead-acid and lithium iron phosphate cells [6], and previous literature has demonstrated experimentally that applying microcycles as a pre-conditioning step also results in improved DCA performance [11].

The cause of this improvement has been investigated by the use of detailed electrochemical simulations of cells, which has shown that this effect is due to the microcyling improving the homogeneity of the current distribution within the cell. This allows for charge to be accepted as efficiently as possible [7]. It has previously been identified by the authors that with microcycles consisting of square-wave like pulses, increasing the frequency of the microcycles results in increased charge acceptance. This paper presents the results of an investigation to determine if the above mechanism may be used to achieve similar improvements in DCA performance by injecting a sinusoidal ripple current at a higher frequency, but of a lesser magnitude than those used in the previous testing.

This approach represents the most practical method of improving charge acceptance in real-world applications. The main benefit of microcycling is that it essentially independent of the battery's current state, and thus can be applied at any point as required. With a balanced microcycle the amount of energy added during charge is equal to that removed during discharge, therefore the overall SoC of the battery remains unchanged. This allows the microcycling to be applied at any SoC, without risking over-charging or -discharging the battery. Microcycling using sinusoidal currents also has the potential to be highly efficient, by using a resonant circuit to produce the ripple current, the energy used is simply cycled between the battery and the reactive components in the resonator; in this approach the total efficiency of the system is primarily governed by the charge efficiency of the battery and the efficiency of the resonator, typically both of these would be better than 95 %.

2. Battery Analysis

The batteries used in this study were RS Pro 698-8091 VRLA type, consisting of six cells in series, with a nominal voltage of 12 V and a rated capacity (C_{nom}) of 4 Ah. To maximise the effectiveness of the applied ripple current and to minimise losses within the battery, it is important that the frequency-dependant behaviour of the battery is understood. Thus, before proceeding to

4

the main testing phase, the batteries were analysed to determine their impedance response across a range of frequencies.

2.1. Spectroscopy

This analysis was performed using a Solartron Analytical 1260 and 1287 Electrochemical Impedance Spectroscopy (EIS) instrument, in conjunction with an environmentally controlled chamber to maintain the ambient temperature of the battery at 25 °C $\pm$ 2 °C throughout the analysis period. This is crucial, as the impedance response is highly dependant on the temperature of the battery.

Prior to performing the analysis on each battery, it was discharged to 70 % SoC, this is the same as that at which the DCA testing was performed (see below for details) and the battery rested. This ensures that the results of the spectroscopy are representative of the performance of the battery during the DCA test, as the frequency response will change with SoC [12]. The analysis was performed with the EIS instrument in potentiostatic mode, after discharging to 70 % SoC the cell was rested for 10 hours to determine the open-circuit voltage (OCV), the test instrument then maintains this OCV potential throughout the test period. Superimposed on the OCV potential is a sinusoidal ac voltage; this causes a current to flow in the battery which is measured by the test instrument. From the applied voltage and measured current the impedance of the battery is determined by the Solartron software. This process is performed repeatedly with the frequency of the applied voltage varying, in this way a spectrum is produced giving the impedance of the battery across a range of frequencies.

For this analysis the frequency range selected was 10 mHz – 1 MHz, using a logarithmic sweep with 20 points per decade. This being selected to be representative of both the low frequency components typical of the DCA test procedure as well as higher frequencies commonly produced by power-electronic switching devices. The range chosen also gives a wide spectrum which allows for a better understanding of the underlying performance of the battery. Figure 1 shows the results of the analysis, with the measured response shown in blue.

From the spectroscopy result it is clear that the behaviour of the battery can be separated into two broad regions. At low frequencies the response is capacitive, as indicated by $Im(Z)$ and the phase angle being negative. Conversely, as frequency increases $Im(Z)$ and the phase angle become positive, indicating an inductive response. The crossover frequency between these two regions occurs at around 1.5 kHz. To better understand the performance of the battery, each region was considered individually for modelling before the two models were combined to produce a full representation of the battery behaviour.
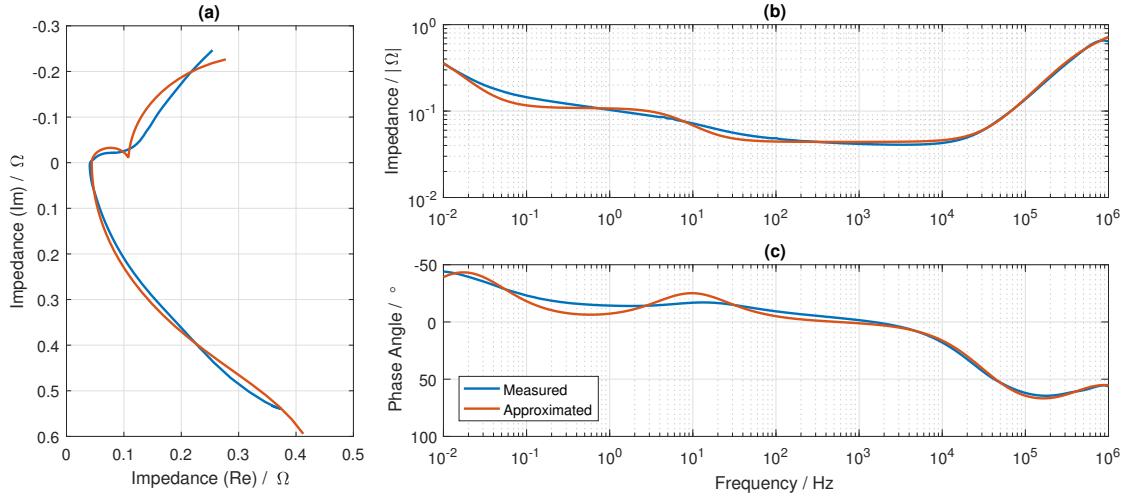
Figure 1: EIS Spectra. (a) Nyquist Plot, (b) Bode Plot - Magnitude Response, (c) Bode Plot - Phase Response

2.2. Modelling

A commonly used electrical model for the low-frequency behaviour of a battery is the Randles model [9], this models the battery as a pair of series connected, parallel RC circuits, as shown in figure 2a. Whilst improvements have been proposed to this model [13], the basic Randles circuit is well regarded for its simplicity.

The software provided with the EIS instrument (*ZPlot & ZView 2*) allows for the fitting of models to measured data. When provided with an equivalent circuit and some initial parameter estimates, the software performs an iterative fitting process to determine the component values
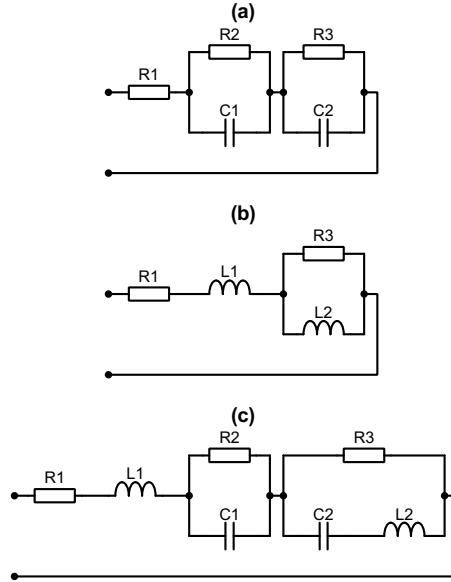

Figure 2: Battery Equivalent Circuit Models. (a) Randles, (b) High frequency from [14], (c) Hybrid

6

which best approximate the measured data; i.e. the smallest weighted error between the measured and approximated frequency spectra. The results of this process for the Randles model applied to the measured frequency spectrum from 10 mHz – 1.5 kHz are given in table 1–A.

A high-frequency variant of the Randles battery model is proposed by [14]. This replaces the capacitive elements of the traditional Randles model with inductors and simplifies the parallel branches, to better represent the electrical behaviour of the battery at higher frequencies. This model is shown in figure 2b, note that the components have been numbered such that those representing the same elements as in the Randles model share their numbers with those from the Randles circuit. The results of the fitting process using this high-frequency model applied to the measured frequency spectrum from 1.5 kHz – 1 MHz are given in table 1–B.

Table 1: Model Component Parameters

Component	Model		
	A	B	C
R_1	46.1 mΩ	41.1 mΩ	44.0 mΩ
R_2	63.7 mΩ	–	64.1 mΩ
R_3	530.0 mΩ	412.6 mΩ	472.0 mΩ
C_1	397.8 mF	–	398.2 mF
C_2	45.0 F	–	45.0 F
L_1	–	66.1 nH	63.5 nH
L_2	–	140.4 nH	141.8 nH

By combining the traditional Randles model with the high-frequency equivalent, it is possible to produce a wide-bandwidth model which can accurately describe the behaviour of the battery across a much wider range of frequencies than would be possible with either model alone. By using the Randles circuit as the basis for this model it can be seen that, despite its simplicity, the proposed hybrid model is a good representation of the true performance of the battery.

It may be seen that the components common to both the models described above, R_1 & R_3, have similar values. This is a good indication that the models are describing the same system but at different frequencies, as the resistive elements should be independent of frequency. Combining both models to produce a hybrid model results in the equivalent circuit given in figure 2c. This is similar to previously described models [12, 15, 16], but with the reactive components replacing constant-phase elements.

Using the component values previously determined as a starting point and the whole measured frequency spectrum, the results of the fitting process for the hybrid model are given in table 1–C. The performance of this hybrid model to the same stimulus as the actual battery is shown by figure 1, in orange. The similarities between the measured and approximated responses are clear

and suggests the model is a reasonable and accurate description of the behaviour of the battery.

2.3. Ripple Frequency Selection

Aside from providing a model describing the behaviour of the battery, the spectroscopy results also allow for the selection of likely frequencies for affecting the performance of the battery. As the hybrid model includes both inductive and capacitive elements, this indicates that the battery will behave in a similar way to a resonant circuit.

As $f \to \infty$ the impedance of the inductors becomes significant and the battery impedance will be dominated by that of L_1, this being in series with all other elements. As $f \to 0$, conversely, the capacitive elements dominate; as these are in parallel branches, the battery impedance will tend toward the sum of R_1, R_2 and R_3. This behaviour can clearly be seen from the measured impedance spectrum in figure 1b, the impedance is relatively high at low frequency; as frequency increases, the impedance falls to a minimum at around 50 Hz. It then remains broadly flat until around 10 kHz, at which point the inductance becomes significant and the impedance rises rapidly.

The main charge storage elements of the battery are modelled by the capacitors, C_2 in particular, therefore in order to affect the performance of the battery as a whole it is important that the ripple current affects these elements. At low frequencies the bulk of the current will flow in the resistances, whilst at high frequencies although C_1 will be the favoured current path through the network of C_1 & R_2, L_2 will restrict current flow through C_2. Therefore, to maximise the current flow through the capacitive elements, the frequency should be be selected to lie in the range at which the total impedance of the battery is at a minimum.

The spectroscopy result given in figure 1b shows the battery impedance to be at a minimum in the range of circa 50 Hz – 10 kHz. From this broad range it is unclear which frequency would be best for influencing the battery. R_1 & L_1 together model the impedance of the internal connections between the terminals and cells within the battery, as such they do not represent the performance of the charge storing structures. By neglecting these components a frequency spectrum for the charge storage elements alone may be produced, as shown in figure 3.

As can be seen, this much more closely resembles the classical resonant circuit impedance spectrum, with a clearly defined resonant frequency of around 700 Hz. This corresponds to the point of minimum impedance, and is therefore selected as the baseline frequency of the ripple current used for the testing described below.

3. Test Procedure

The test procedure is based on previous work by the authors to determine how DCA performance is influenced by the test parameters, this work is reported in [6].
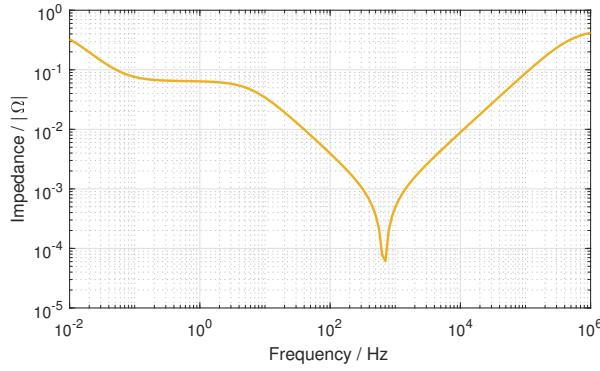
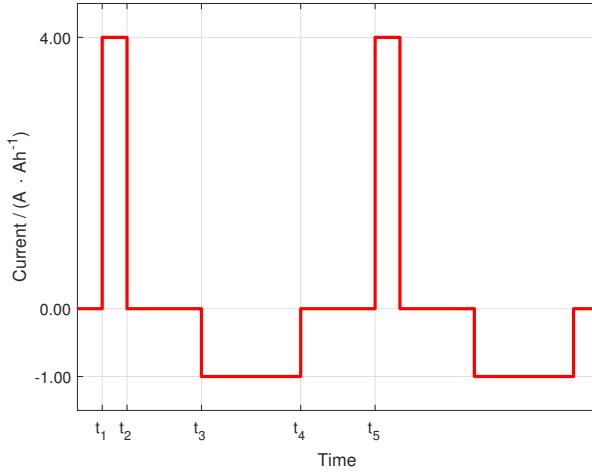Figure 3: Impedance Spectrum for Hybrid Model, Neglecting R_1 & L_1

Figure 4: DCA Test Microcycle Current Profile $(t_1 - t_5)$

3.1. DCA Description

A full discussion of the DCA test procedure is beyond the scope of this paper, for full details see [5, 6]. Briefly, however, at the core of the DCA test is the DCA microcycle. This is a specified current waveform which is applied to the battery, from its response to this stimulus the DCA performance may be determined. The microcycle used for this test, as modified from the DCA Test standard is shown in figure 4 and summarised in table 2.

All currents applied during the test procedure are normalised to the capacity of the battery, and as such are expressed in terms of A·Ah^{-1}, which may also be expressed as C A.

The key part of the microcycle is step 1, here the test applies a large charge pulse to the battery, causing its voltage to rise. If the voltage exceeds 14.8 V, the charge current is reduced to maintain the voltage at the upper limit. This reduction in charge current will equate to a lower total amount of charge accepted for the microcycle. DCA is determined by the amount of charge the battery is able to accept as a fraction of the total amount theoretically available. The current levels used for the microcycle are normalised to the actual capacity of the battery C_{exp}, which is

9

Table 2: DCA Test Microcycle Current Profile Procedure

Step	Description
1, $(t_1 - t_2)$	Charge at 4.00 A·Ah^{-1} with voltage limit of 14.8 V for 10 s
2, $(t_2 - t_3)$	Rest 300 s
3, $(t_3 - t_4)$	Discharge at 1.00 A·Ah^{-1}
4, $(t_4 - t_5)$	Rest 300 s

experimentally determined by the test procedure.

Each microcycle is charge-balanced, the amount of charge added to the battery in step 1 is removed during step 3, i.e:

$$\int_{t_1}^{t_2} I(t) \ dt = - \int_{t_3}^{t_4} I(t) \ dt \tag{1}$$

This is achieved by dynamically varying the length of the discharge step, and ensures that the SoC at the end of the microcycle is the same as it was at the start. The remaining sections of the microcycle run for fixed times as specified in table 2. The battery is subjected to 20 repetitions of the microcycle profile, this being one DCA Pulse Profile (DCAPP).

3.2. DCA Calculation

DCA is given in terms of the average recuperation current (I_{recu}) for the charge pulse [8], which has units of A·Ah^{-1}. Thus, for a pulse of arbitrary length, DCA is given by

$$I_{recu} = \frac{Ah_{recu} \cdot 3600}{C_{exp} \cdot t} \tag{2}$$

where Ah_{recu} is the amount charge accepted during the pulse in ampere-hours, C_{exp} is the capacity of the battery in ampere-hours and t is the length of the charge pulse in seconds.

3.3. Effect of History on DCA Performance

A critical factor influencing DCA performance, as identified by [6], is the operational history of the battery. This refers to the operations which have been performed on the battery prior to the DCA test and may be divided into discharge history (DH), where the battery has previously been discharged, and charge history (CH) where it was charged.

The effects of this history have been shown by [6] to be very significant, with large differences in DCA performance at the same SoC, dependant on the battery's history. It is crucial therefore that this influence be accounted for in the test procedure.

3.4. Test Rig

To perform the necessary testing, a custom test rig was constructed. This is shown, in overview, in figure 5, and consists of two current sources connected to the battery under test. This approach allowed for the ac ripple current to be applied independently of the dc currents used during the DCA test and to charge and discharge the battery.

The dc current source is provided by a MACCOR Series 4000 battery test system, this is a commercial unit which is designed for the reliable and efficient testing of batteries. In this case the unit was configured to provide a maximum, bi-directional dc current of 20 A at up to 20 V. The system has the ability to log data during the testing process, in this case the tester was configured to log the dc battery current and voltage. The analogue signals were pre-filtered to remove the effects of the ac ripple before being passed to the MACCOR system for logging.
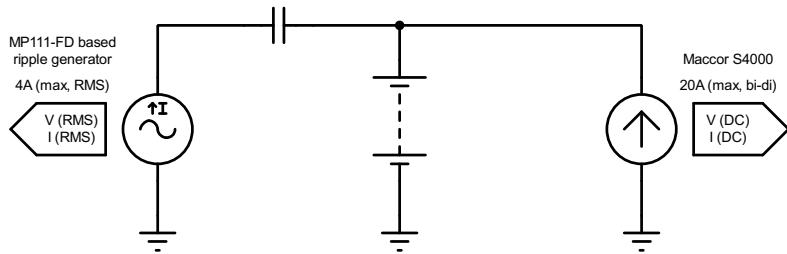

Figure 5: Test Rig Overview

To produce the necessary ac ripple current, a bespoke ripple generator was constructed. This is based around the Apex Microtechnology MP111-FD Power Operational Amplifier, which was chosen for its wide power bandwidth and high current output. As constructed the generator is capable of producing ripple currents up to 4 A_{RMS} across a frequency range from 100 Hz – 180 kHz, and contains the required circuitry to produce analogue outputs scaled to the RMS values of the generated current and voltage. These signals were fed into axillary inputs on the MACCOR system, so all logging and data storage was centralised.

The ac ripple current is capacitively-coupled onto the dc bias current, this eliminates the need for voltage matching between the generators and ensures the ripple current present on the battery is always superimposed on top of the existing dc voltage.

3.5. Test Description

Figure 6 shows the SoC profile for the test procedure. This begins with a high-rate discharge to test the reserve capacity of the battery, followed by a 1-hour rest and recharge to 100 % SoC. The battery is then discharged to 0 % SoC at the 5-hour rate, from this C_{exp} is determined. From this point the battery is then fully recharged, rested and discharged to 70 % SoC. Following another 1-hour rest the first DCAPP is performed, this testing the DCA performance when the battery
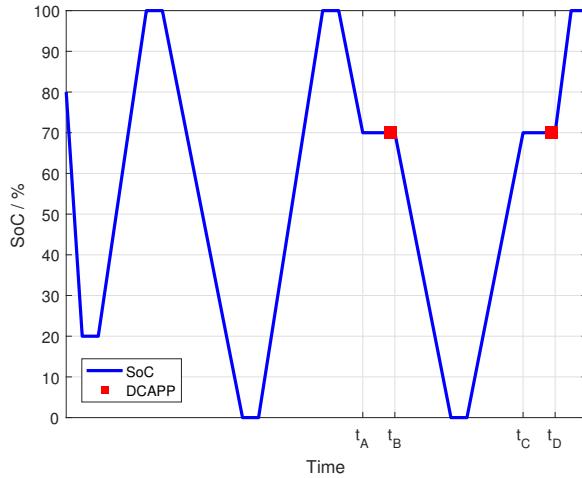
Figure 6: Test Procedure SoC Profile & DCAPP Locations

has discharge history. For the duration of the DCAPP and the rest period leading up to it (t_A – t_B), a sinusoidal ripple current of 1.6 A$_{RMS}$, equivalent to $0.4C_{nom}$, at 700 Hz is applied to the battery.

The battery is then fully discharged, rested and recharged to 70 % SoC. Again, after resting for 1-hour a second DCAPP is performed, testing the DCA performance with charge history. As before the ripple current is applied for the duration of the DCAPP procedure and the rest preceding it, t_C – t_D. Figure 7 shows an enlargement of the time around the DCAPP, allowing the SoC and ac and dc currents to be seen in more detail.

4. Results & Discussion

The initial testing focussed on the effect of ac ripple at a frequency of 700 Hz, as identified by the battery characterisation above, later in this paper this will be extended to include the effect of varying ripple frequencies. To establish a baseline performance, the test procedure described above was applied to the battery under test, but without any injected ripple. The battery performance under these conditions is shown in figure 8, in blue. This figure shows the average charge acceptance for each of the 20 microcycles of the DCAPP, with charge and discharge history, this shows the typical DCA performance traits as identified by [6].

The first and most obvious of these is the large difference in performance dependant on the operational history of the battery; with discharge history the performance is significantly better than when the battery has charge history. Secondly, the history influences the performance as the DCAPP progresses in different ways, with discharge history there is a general decrease in charge acceptance as the number of microcycles increases, whilst with charge history the performance is broadly consistent across the whole DCAPP.
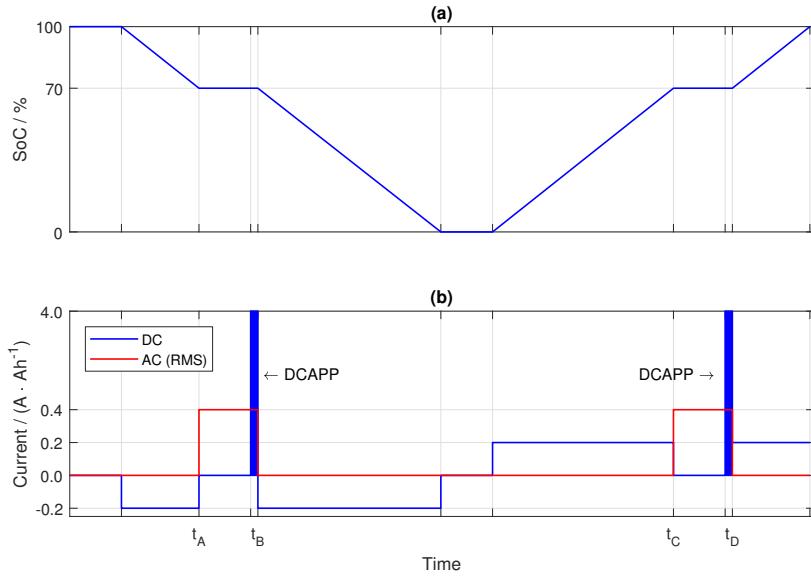
12

Figure 7: Test Procedure Details. (a) SoC Profile, (b) Applied Current Profile

4.1. Effects of 700 Hz Ripple

Figure 8 also shows the DCA performance of the battery when subjected to the full test procedure with the 1.6 A_{RMS}, 700 Hz ripple current applied. It may be clearly seen from this figure that the injection of a ripple current improves the charge acceptance performance of the battery. The result shows the same traits as identified for the baseline are present, but in all cases the amount of charge accepted is greater.

This differs from the effect previously observed when the rest period within the DCAPP was reduced, in those cases whilst DCA performance was improved, the trend of charge acceptance within the DCAPP was also altered; tending to increase as the number of microcycles increased [6].
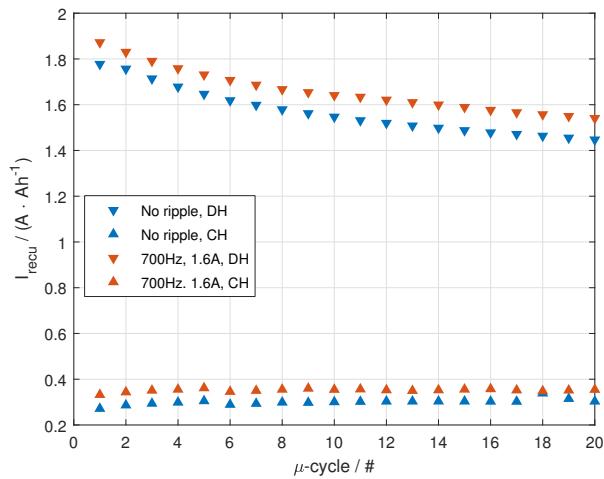

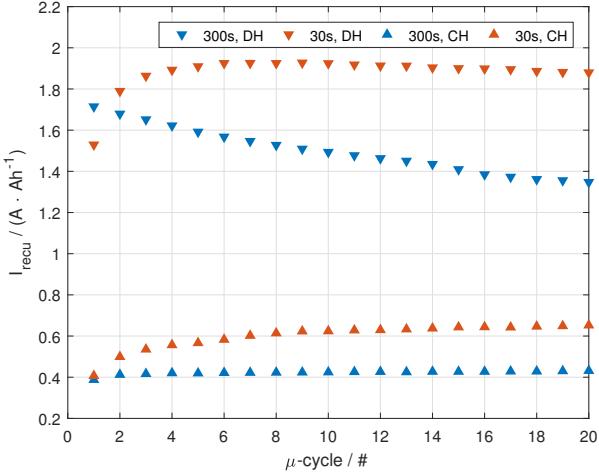Figure 8: DCA Analysis Result - Effect of Injected Ripple Current

13

Figure 9: DCA Analysis Result - Effect of Reduced Rest Period

This is illustrated by figure 9, which shows the effect on the DCA performance of a VRLA cell when the rest period is reduced from 300s as used in this test, to 30s; the data being taken from [6].

Comparing the results given in figure 9 with those observed from this study (figure 8), it may be seen that the effect produced by the injected ripple current is very different to that caused by reducing the rest period. Whilst both methods improve DCA performance, the injected ripple current does not alter the trend of charge acceptance within the DCAPP as reducing the rest period does.
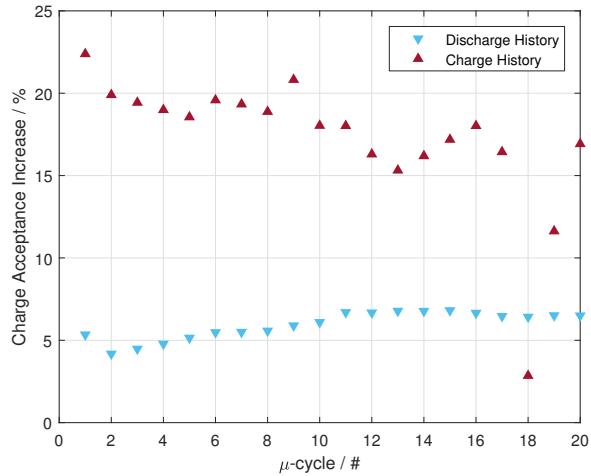

Figure 10: Charge Acceptance Improvement with Applied 700 Hz Ripple Current

The magnitude of the improvement seen is illustrated by figure 10, which shows the percentage increase in charge acceptance over the baseline for each microcycle. This result is of particular interest as it shows a significantly larger improvement in performance when the battery has charge history, this is important as the overall charge acceptance is much poorer in this case, so this larger

14

improvement will be more beneficial to the performance of the battery. For completeness, table 3 gives the average performance improvement for the compete DCAPP observed in this study.

Table 3: Average Charge Acceptance Improvement with Applied Ripple Current

History	Increase
Discharge	5.94 %
Charge	17.24 %

4.2. Effect of Varying Frequency

The above result shows that an injected ac ripple current can increase charge acceptance, from previous work it was observed that increasing the frequency of the microcycles used within the DCA test also increased charge acceptance. To examine whether this trend continued with ac ripple currents, the investigation was extended to consider frequencies higher than 700 Hz. Three additional frequencies were selected, these being approximately evenly spaced – on a logarithmic scale – between 700 Hz and the maximum achievable from the test rig; the resultant frequencies were 4.5 kHz, 30.0 kHz and 180.0 kHz. Consideration was given to investigating frequencies below 700 Hz, but with the rig being capable of a minimum of only 100 Hz, it was felt that this would add little to the results.
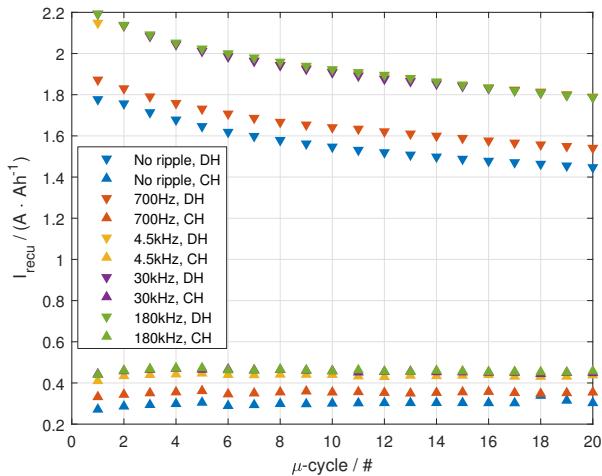

Figure 11: DCA Analysis Result - Effect of Injected Ripple Currents of Various Frequencies

The test procedure described above was repeated at each of the frequencies of interest, the result of this testing is shown in figure 11, with the baseline result and that at 700 Hz included for clarity. From these results it is clear that moving to higher frequencies does improve charge acceptance, furthermore it can be seen that, as at 700 Hz, the trend in DCA performance throughout the DCAPP follows that of the baseline. This is important as it suggests that whilst the injected ripple improves the battery's charge acceptance it does not significantly alter its other behaviour.
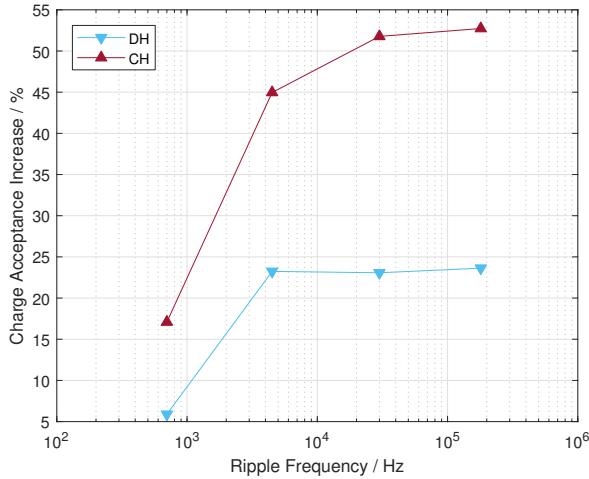
Figure 12: Average Charge Acceptance Improvement with Applied Ripple Currents

Figure 12 shows the average increase in charge acceptance for the whole DCAPP over the baseline, for each frequency of interest. This clearly demonstrates the benefits of increasing ripple frequency as charge acceptance improvement increases from around 6 % and 17 % with discharge and charge history respectively at 700 Hz to 24 % and 53 % at 180 kHz. It is also interesting to note that the increase is not linear, rather most gains are achieved with the initial increase from 700 Hz to 4.5 kHz. This is particularly true for discharge history, which showed virtually no additional improvement beyond this point. In the case of charge history, further improvement was observed but at a far lesser degree than previously, and by 180 kHz this too shows virtually no increase in performance with increased ripple frequency.

Aside from the obvious charge acceptance increases, moving to higher ripple frequencies brings other benefits. Firstly, for a given power-rating the size of the reactive components required in generating the ripple current is reduced as frequency increases. This provides benefits in terms of material cost and size constraints. A secondary advantage of moving to higher frequencies is that the ripple frequency can be above 20 kHz, which is the upper limit of human hearing, by going above this frequency the ripple generator will produce no audible emissions.

There are however disadvantages to higher frequency operation. As the impedance of the battery increases with frequency, generating ripple currents at higher frequencies requires more power and will increase the losses within the system. This is illustrated by table 4 which shows the battery impedance for each frequency of interest and the relative power required to generate a ripple of a given current over that at 700 Hz.

Clearly, there is a trade-off to be made between the benefits of higher frequency ripple in terms of charge acceptance and the disadvantages of much increased power requirements. In this case it would appear that operation around the 30 kHz mark would provide an acceptable solution.

16

Table 4: Battery Impedance and Power Requirements for Various Frequencies of Ripple Current

Frequency	Impedance (mΩ)	Power
700 Hz	42.25	–
4.5 kHz	40.87	0.97
30 kHz	60.72	1.44
180 kHz	222.20	5.26

4.3. Analysis of Varying Frequency

The result described above demonstrates that increasing the ripple current frequency above 700 Hz improves DCA performance, it is therefore apparent that the impedance analysis presented in figure 3 is not sufficient, on its own, to fully describe the behaviour seen. By performing ac circuit analysis techniques on the equivalent circuit model given in figure 2c it is possible to calculate the current which will flow in any given component for a given ripple current frequency as a proportion of the total current applied to the terminals of the circuit.

As the charge-storing elements of the circuit are of paramount interest in this case, these elements (C_1 & C_2) have been chosen as the subjects of this analysis, the result of which is given in figure 13.
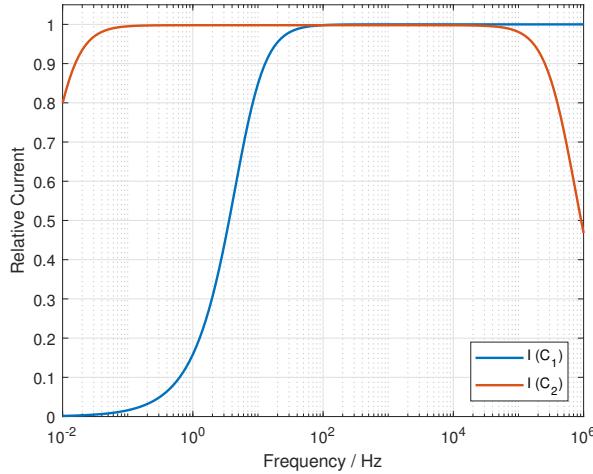

Figure 13: Current Distribution in C_1 & C_2 with Frequency

This clearly shows how the applied ripple current is distributed within the battery. C_1 sees very little current at low frequencies, however this rapidly increases with frequency to reach a point at which virtually all applied current passes through C_1 for frequencies above 100 Hz. C_2 starts with a much greater proportion of the current, and like C_1 soon reaches a point where it is carrying all the applied current. At very high frequencies, however, the effects of the inductor in series with C_2 begin to show and the relative current reduces as frequency continues to increase

17

above 50 kHz.

To fully describe the behaviour seen, it is important to understand what C_1 and C_2 represent in terms of the physical aspects of the battery. C_2 is representative of the main electrochemical charge storage element of the cell, hence its large capacitance, whilst C_1 models the transient effect of changing current densities and ion concentrations on the surface of the electrodes of the battery [13]. The nature of the DCA test makes it essentially a test of the surface capacitance of the battery, as the short, high-current pulses applied primarily affect only the surface of the electrodes. Therefore it may be seen that in order to improve DCA performance it is important that C_1 in particular is effected by the applied ripple current.

Previous work by the authors has shown experimentally that reducing the rest periods within the DCA test, and thus increasing the frequency of the current pulses, improves DCA performance [6]. Simulations show that these microcycles improve the homogeneity of the current distribution across the electrodes of the battery and allow for more efficient charge acceptance [7]. The results of this work show that such an effect may also be achieved with the use of high-frequency ripple currents and the behaviour seen may be clearly explained considering the results from figure 13.

For frequencies above 100 Hz, all applied ripple currents pass through C_1, where they are able to influence the current distribution. That DCA performance improves with increasing frequency is as a result of the higher frequencies promoting a greater level of homogeneity within the battery. It is also not surprising that the improvement in performance begins to level-off at around the 50 kHz point, as there will be an upper limit to the improvement achievable, whereby even with perfectly evenly distributed current the battery cannot physically accept charge any more efficiently.

4.4. Effect of Ripple Current on SoC

A major potential drawback of the use of ripple currents of any frequency is the effect on the SoC of the battery. As the round-trip efficiency of the battery is less than 100 %, not all of the energy removed during the negative half-cycle will be returned during the positive half, even if the currents in both are equal. Whilst the net loss of charge per cycle will be negligible, over time the cumulative effect could produce a significant reduction of SoC.

Were this to be the case, it would add significant complexity to the system. Either the battery management system (BMS) would need to measure and account for the loss, which would require the use of high-frequency measuring equipment, adding to the cost of the BMS, or the ripple generator would need to produce a ripple with a dc offset to compensate for the loss of SoC, again adding significant complexity and cost.

To asses the effect of injected ripple currents on SoC a second test procedure was devised. In this, a fully charged, well-rested battery was discharged to 70 % SoC. It was then allowed to

rest, open-circuit, for five days whilst its open-circuit-voltage (OCV) was logged every 10 seconds. This measured voltage profile was used as a baseline, against which the effect of the ripple current could be assessed. The test was then repeated, but in this case as soon as 70 % SoC was reached and the dc bias current was removed, an ac ripple current was applied for five days. During this period the terminal voltage of the battery was again measured every 10 seconds. In this way, were the ripple current to have an effect on the SoC of the battery it would be shown by a deviation in the voltage profile from that of the baseline. The two extremities of the previously explored ripple frequencies were tested, 700 Hz and 180 kHz.
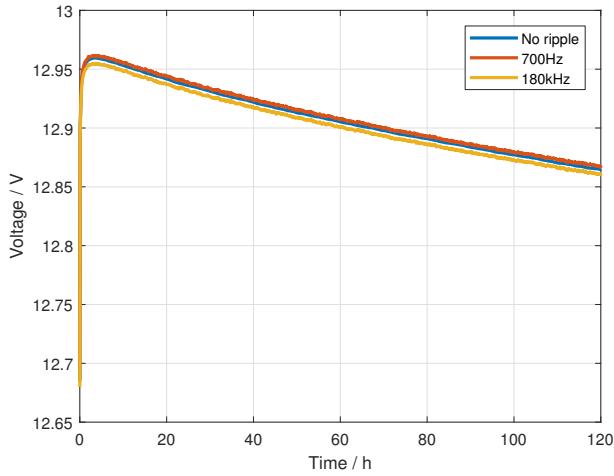

Figure 14: Voltage Profiles from 5-day SoC Test

Figure 14 shows the results of this testing. From this it is clear that the presence of the ripple currents has no appreciable effect on the SoC of the battery, all three curves follow identical patterns, the only differences being due to a slight variation in the initial voltage. Table 5 summarises the starting and ending voltages for the test, it may be seen that there was a difference of only 1 mV between the tests with ripple present and the baseline. This is well within the noise of the data and clearly shows that even after five days the presence of the ripple currents has not appreciably discharged, or indeed charged, the battery, and has thus not altered its SoC.

Table 5: Battery Start, End and ΔV Voltages from 5-day SoC Test

Frequency	Start (V)	End (V)	ΔV (V)
No ripple	12.685	12.865	0.180
700 Hz	12.687	12.868	0.181
180 kHz	12.680	12.861	0.181

5. Conclusions

The work has shown that the application of ac ripple currents to lead-acid batteries can significantly improve their DCA performance by increasing the homogeneity of the current distribution within the battery and thus improving the efficiency of charge acceptance. Improvements in charge acceptance of over 50 % have been seen, with the use of ripple currents of only 0.4 C. The improvements have been observed across a wide range of frequencies, and are seen to become greater as frequency is increased. The increase is not linear, however, and moving to frequencies greater than 30 kHz provides little benefit; especially when the increasing power requirements due to increased battery impedance are considered. The application of sinusoidal ripple currents does not appear to measurably alter the SoC of the battery, even after periods as long as five days.

References

[1] M. Ehsani, Y. Gao, J. M. Miller, Hybrid electric vehicles: architecture and motor drives, Proceedings of the IEEE 95 (4) (2007) 719–728. `doi:10.1109/jproc.2007.892492`.

[2] C. Chumchal, D. Kurzweil, Lead–acid battery operation in micro-hybrid and electrified vehicles, in: Lead-Acid Batteries for Future Automobiles, Elsevier, 2017, pp. 395–414.

[3] P. T. Moseley, D. A. Rand, Partial state-of-charge duty: A challenge but not a show-stopper for lead-acid batteries!, ECS Transactions 41 (13) (2012) 3–16. `doi:10.1149/1.3691907`.

[4] E. Karden, S. Ploumen, B. Fricke, T. Miller, K. Snyder, Energy storage devices for future hybrid electric vehicles, Journal of Power Sources 168 (1) (2007) 2–11. `doi:10.1016/j.jpowsour.2006.10.090`.

[5] European Committee for Electrotechnical Standardisation, EN 50342-6:2015. Lead-acid starter batteries - Part 6: Batteries for Micro-Cycle Applications (November 2015).

[6] M. Smith, D. Gladwin, D. Stone, Experimental analysis of dynamic charge acceptance test conditions for lead-acid and lithium iron phosphate cells, Journal of Energy Storage 12 (2017) 55–65.

[7] J. Kowal, D. Schulte, D. U. Sauer, E. Karden, Simulation of the current distribution in lead-acid batteries to investigate the dynamic charge acceptance in flooded sli batteries, Journal of Power Sources 191 (1) (2009) 42–50. `doi:10.1016/j.jpowsour.2008.12.016`.

[8] H. Budde-Meiwes, D. Schulte, J. Kowal, D. U. Sauer, R. Hecke, E. Karden, Dynamic charge acceptance of lead–acid batteries: Comparison of methods for conditioning and testing, Journal of Power Sources 207 (2012) 30–36. `doi:10.1016/j.jpowsour.2011.12.045`.

[9] K. Vetter, Elektrochemische Kinetik. (German) *[Electrochemical Kinetics]*, Springer, Berlin, 1961.

[10] M. Thele, J. Schiffer, E. Karden, E. Surewaard, D. Sauer, Modeling of the charge acceptance of lead–acid batteries, Journal of Power Sources 168 (1) (2007) 31–39.

[11] D. U. Sauer, E. Karden, B. Fricke, H. Blanke, M. Thele, O. Bohlen, J. Schiffer, J. B. Gerschler, R. Kaiser, Charging performance of automotive batteries—an underestimated factor influencing lifetime and reliable battery operation, Journal of power sources 168 (1) (2007) 22–30.

[12] S. Buller, M. Thele, R. W. De Doncker, E. Karden, Impedance-based simulation models of supercapacitors and li-ion batteries for power electronic applications, in: Industry Applications Conference, 2003. 38th IAS Annual Meeting. Conference Record of the, Vol. 3, IEEE, 2003, pp. 1596–1600.

[13] C. R. Gould, C. M. Bingham, D. A. Stone, P. Bentley, New battery model and state-of-health determination through subspace parameter estimation and state-observer techniques, Vehicular Technology, IEEE Transactions on 58 (8) (2009) 3905–3916. `doi:10.1109/TVT.2009.2028348`.

[14] J. Wang, K. Zou, C. Chen, L. Chen, A high frequency battery model for current ripple analysis, in: Applied Power Electronics Conference and Exposition (APEC), 2010 Twenty-Fifth Annual IEEE, IEEE, 2010, pp. 676–680.

[15] D. A. Howey, P. D. Mitcheson, V. Yufit, G. J. Offer, N. P. Brandon, Online measurement of battery impedance using motor controller excitation, IEEE transactions on vehicular technology 63 (6) (2014) 2557–2566.

[16] D. Howey, V. Yufit, P. Mitcheson, G. Offer, N. Brandon, Impedance measurement for advanced battery management systems, in: Electric Vehicle Symposium and Exhibition (EVS27), 2013 World, IEEE, 2013, pp. 1–7.